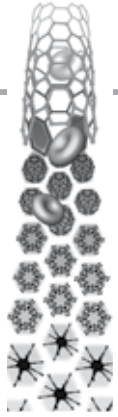

Intranasal administration of antiretroviral-loaded micelles for anatomical targeting to the brain in HIV

We investigated the intranasal administration of poly(ethylene oxide)–poly(propylene oxide) polymeric micelles loaded with high payloads of the first-line antiretroviral drug efavirenz for targeting to the CNS. The effect of micellar size and composition and drug payload was assessed, employing simple micelles made of a highly hydrophilic copolymer, poloxamer F127, loaded with 20 mg/ml drug and mixed micelles containing 75% of a medium hydrophobic poloxamine, T904, and 25% F127 loaded with 20 and 30 mg/ml drug, respectively. F127 confers high physical stability, while T904 substantially improves the encapsulation capacity of the micelles. The bioavailability of the drug in the CNS was increased fourfold and the relative exposure index (ratio between the area-under-the-curve in the CNS and plasma) was increased fivefold with respect to the same system administered intravenously. These findings demonstrate the potential of this scalable and cost-viable strategy to attack the HIV sanctuary in the CNS.

KEYWORDS: anatomical targeting to the brain ■ CNS ■ efavirenz-loaded micelles ■ HIV reservoirs ■ intranasal administration

Diego A Chiappetta[1,2], Christian Hocht[3], Javier AW Opezzo[3] & Alejandro Sosnik*[1,2]

[1]The Group of Biomaterials & Nanotechnology for Improved Medicines (BIONIMED), Department of Pharmaceutical Technology, Faculty of Pharmacy & Biochemistry, University of Buenos Aires, 956 Junín St., 6th Floor, Buenos Aires CP1113, Argentina
[2]National Science Research Council (CONICET), Buenos Aires, Argentina
[3]Department of Pharmacology, Faculty of Pharmacy & Biochemistry, University of Buenos Aires, Argentina
**Author for correspondence:*
Tel.: +54 11 4964 8273
Fax: +54 11 4964 8273
alesosnik@gmail.com

The HIV epidemic affects approximately 35–40 million people [101]. Highly active antiretroviral therapy has prolonged the lifespan and improved the quality of life for patients infected with HIV [1]. Therapeutic success relies on the chronic administration of a minimum of three antiretrovirals (ARVs) belonging to different families [2]. However, highly active antiretroviral therapy does not eradicate HIV from the host, owing to the generation of intracellular and anatomical reservoirs, where the virus remains latent (and insensitive to the therapy) or less accessible to ARVs due to the presence of different barriers [3–5].

The blood–brain barrier (BBB) is a complex structure that isolates the brain parenchyma from the systemic circulation and represents the main hurdle towards the attainment of therapeutic drug concentrations in the CNS [6].

One of the mechanisms that prevents the appropriate biodistribution of ARVs stems from the activity of transmembrane proteins of the ATP-binding cassette (ABC) superfamily that pump drugs out of viral reservoirs against a concentration gradient [7,8]. P-glycoprotein and breast cancer resistance protein (BCRP) are the most investigated ABCs. Most ARVs are substrates of at least one ABC [9,10]. Their extensive distribution in the BBB leads to subtherapeutic concentrations in the cerebrospinal fluid and in cerebral cells [12] and contributes to the generation of one of the most challenging HIV reservoirs [8,13,14].

The presence of the HIV in the CNS serves as a viral pool but it may also contribute to its progressive deterioration, a disease generally referred to as HIV-associated neurocognitive disorder [12,15–17]. HIV-associated neurocognitive disorder is more frequent in neonates and children and may lead to cognitive, motor, behavioral and developmental sequelae [18]. Until a cure is found, a more effective pharmacotherapy that reduces significantly reduces the viral load in the CNS would improve the course of the HIV-associated neuropathogenesis [15,19].

Different nanotechnologies have been explored to target ARVs to the HIV reservoir in the CNS [20,21]. ARV-loaded polymeric and lipid nanoparticles (NPs) improved drug passage across endothelial cell monolayers (a model of the BBB) by means of passive targeting [22–24]. On the other hand, *in vitro* uptake assays are of relatively limited clinical relevance and their fate upon intravenous (iv.) administration could only be assessed in preclinical studies. ARV-loaded nanocarriers conjugated with transferrin exploited the presence of transferrin receptors on the apical zone of brain endothelial cells [25]. Other strategies comprised the coadministration of the ARV with poly(ethylene oxide)–poly(propylene oxide) (PEO–PPO) block coplymers that inhibit the activity of ABCs [26,27] and cell delivery therapies [28]. The use of expensive ligands and complex synthetic pathways may increase the cost of the medication and

Future Medicine part of fsg

curtail patient affordability in resource-limited countries [29,30].

Polymeric micelles are among the most versatile nanotechnologies to enhance the bioavailability of poorly water-soluble drugs [31]. Linear and branched PEO–PPO block copolymers are among the most popular micelle-forming copolymers [32]. In general, they display good cyto- and biocompatibility [33–35] and some of their derivatives have been approved as pharmaceutical excipients by the US FDA and the EMA.

Efavirenz (EFV) is a highly hydrophobic (log P = 5.4; intrinsic water solubility of 4 μg/ml) first-line non-nucleoside reverse transcriptase inhibitor [36]. The oral bioavailability of EFV ranges between 40 and 45% and it displays an intra- and inter-individual variability of 19–24% and 55–58%, respectively [36]. The EFV half-life is 52–76 h after a single dose and 40–52 h under a chronic regimen [37]. Thus, the EFV dose is between 200 and 600 mg in children (depending on the body weight/surface) and 600 mg in adults once a day; this dose ensures therapeutic plasma concentrations between 1 and 4 μg/ml [38]. EFV is usually taken at bedtime to minimize its psychological and CNS adverse effects [39]. Generally, treatment failure and CNS side effects are associated with low and high EFV plasma levels, respectively. EFV is a substrate of BCRP in the GI tract and brain of rats [40,41].

Different research groups aimed to improve the biopharmaceutic properties of EFV by means of nanotechnology [42–44]. We comprehensively investigated the capacity of pristine and chemically modified PEO–PPOs of different molecular weight, hydrophilic–lipophilic balance and architecture to encapsulate and release EFV [45–49]. The aqueous solubility was increased up to 34 mg/ml (8400-fold) and EFV-loaded micelles resulted in a significant increase of the oral bioavailability in an animal model [45,46].

The exposure of the intranasal (in.) mucosa to environmental NPs and contaminants and their effect on the CNS revealed the presence of a direct nose-to-brain transport pathway [50,51]. Different mechanisms have been proposed, though the transcellular pathway appears as the most relevant, while the paracellular mechanism is less investigated [50]. Thus, drug-loaded nanocarriers would be internalized by terminals of the olfactory and trigeminal nerve systems that begin in the brain and end at the olfactory neuroepithelium and respiratory epithelium, respectively [50]. Thus, intranasal (in.) administration of NPs bypasses the BBB, enhancing the bioavailability of drugs in the CNS. Although the first reports stated 100 nm as the upper limit to capitalize on this route, more recent studies showed that larger NPs (~300 nm) administered in. can also reach the CNS [52]. The main advantages of this route of administration are minimal invasiveness, painlessness, self-administration and high patient compliance. A number of research groups have recently reported on the in. administration of polymeric NPs loaded with different drugs, among them ARVs [53–55]. For example, Mainardes *et al.* delivered the nucleoside reverse transcriptase inhibitor zidovudine, the first FDA-approved ARV, employing PLA and PLA–PEG blend NPs [54]. The systemic bioavailability was increased with respect to a solution. However, the pharmacokinetics (PKs) of the drug in the CNS was not assessed. Al-Ghananeem *et al.* passively targeted another nucleoside reverse transcriptase inhibitor, didanosine, to the brain by the in. administration of drug-loaded chitosan NPs [55]. In both cases, the drugs were water-soluble. Only a few reports described the in. administration of drug-loaded polymeric micelles [56].

Owing to the small volume that can be administered per nostril, only highly concentrated systems can be employed to attain sufficiently high doses; this is one of the main limitations that has likely precluded its translation into clinics [57].

Since PEO–PPO polymeric micelles displayed good encapsulation capacity of EFV with a relatively small change in micellar size [45,46] and no irritation of mucosas [58], they emerge as an excellent platform to target ARVs to the CNS.

In this context, the present work investigated for the first time the PKs of EFV in the CNS upon in. administration and compared it with that of the same systems administered iv.

Materials & methods

Materials

Poloxamer Pluronic® F127 (molecular weight 12.6 kDa, 70 wt% PEO) and poloxamine Tetronic® T904 (T904, molecular weight 6.7 kDa, 40 wt% PEO) were donated by BASF (Florham Park, NJ, USA). EFV (LKM Laboratories, Buenos Aires, Argentina), Na_2HPO_4, citric acid, KH_2PO_4, NaOH, HCl and solvents of analytical grade were used as received.

Preparation of EFV-free & EFV-loaded poloxamine micelles

In general, polymeric micelles (10% final polymer concentration, expressed in weight per volume) were prepared by dissolving the

required amount of copolymer in phosphate buffer solution (PBS, pH 7.4) at 4°C. Pure F127 (1 g) was dissolved in PBS to a final volume of 10 ml. Similarly, for F127:T904 (25:75) mixed micelles, F127 (0.25 g) and T904 (0.75 g) were dissolved in PBS to a final volume of 10 ml [48]. Micelles were equilibrated at 25°C at least 24 h before encapsulation of the drug. To prepare EFV-loaded micelles (20 and 30 mg/ml), 60 or 90 mg of EFV was added to 10% pure or mixed micelles (3 ml) and shaken (25°C, Minitherm-Shaker; Adolf Kuhner AG, Switzerland) until total drug dissolution (2 h). The encapsulation process relies on the incorporation of hydrophobic drug molecules into the micellar core. In preliminary studies conducted when the encapsulation capacity of each micellar system with respect to a drug is unknown, the drug is added in excess and the system shaken until the equilibrium is reached [45–48]. Then, the drug that was not encapsulated and remained in suspension (as magnetic stirring is not energetic enough to break the drug down into pure drug NPs) is removed by filtration (0.45 µm). Once the encapsulation capacity of a specific micellar system was established (shown in preliminary studies) [45–48], the amount of drug used is equal or smaller than that capacity. The former results in drug-undersaturated micelles, while the latter in saturated micelles. Regardless of the micellar system, there is always an amount of drug that is solubilized in water in the free-form (not encapsulated), this value being defined by the drug's intrinsic solubility. In this work, the final systems contained free drug solubilized in water (4 µg/ml) and the rest (up to 20 or 30 mg/ml) encapsulated within the micelles. In this context, the encapsulation efficiency was approximately 100% (e.g., in the case of systems with an EFV concentration of 20 mg/ml, the intrinsic solubility represented only 0.02% of the total drug amount and the rest of drug [99.98%] was solubilized within the polymeric micelles). Pure F127 and mixed F127:T904 (25:75) 10% micelles containing a drug payload of 20 mg/ml are denoted pF127–20 and F127:T904–20, respectively, while F127:T904 (25:75) micelles containing 30 mg/ml of EFV are named F127:T904–30.

Micellar size, size distribution, morphology & physical stability

The average hydrodynamic diameter (D_h) and size distribution of EFV-loaded micelles in different aqueous media were measured by dynamic light scattering (Zetasizer Nano-Zs, Malvern Instruments, Worcestershire, UK) provided with a He-Ne (633 nm) laser and a digital correlator ZEN3600, at 25°C. Measurements were conducted at a scattering angle of $\theta = 173°$ to the incident beam. Results of D_h and polydispersity index are expressed as the mean ± standard deviation of three independent samples prepared under identical conditions. Data for each single sample was the result of at least five runs.

The morphology of pF127–20 micelles was studied by transmission electron microscopy (EM 109T Zeiss Transmission Electron Microscope, Karl Zeiss, Berlin, Germany). The sample (5 µl) was placed onto a copper grid covered with Fomvar film and stained with phosphotungstic acid (5 µl, 2% w/v water solution). Finally, the sample was dried in a closed container with silica gel and visualized.

To assess the physical stability of the micelles under plasma-mimicking conditions, samples were diluted (1/20) in PBS with bovine serum albumin (1 and 3%; Sigma-Aldrich) and the size and size distribution monitored over 24 h, at 37°C.

Animal preparation

Male 3-months-old Wistar rats were used (250–270 g). Each experimental group comprised of six animals. Animals were maintained on a 12 h light/dark routine at 22 ± 2°C with the air adequately recycled. They received a standard rodent diet (Asociación Cooperativas Argentinas, Buenos Aires, Argentina) with the following composition (w/w): 20% protein, 3% fat, 2% fiber, 6% mineral, and 69% starch and vitamin supplements. Experiments were conducted in fasted (12 h) and anesthetized rats (see below). After the experiments, anesthetized animals were euthanized by decapitation.

EFV dosing

The concentration of EFV in the CNS after iv. and in. administration of the different EFV-loaded micelles was monitored by microdialysis. This methodology enables the continuous assessment of extracellular drug concentrations in a specific nucleus [59]. Concentric microdialysis tube semipermeable membranes produced in our laboratory [60] were inserted into the anterior hypothalamus by means of stereotaxy (A/P-1.7 mm, L/M-0.8 mm, V/D-9.5 mm, from the bregma) of male Wistar rats anesthetized with a combination of urethane (500 mg/kg)/chloralose (50 mg/kg). Upon insertion, the dialysis membrane was equilibrated for 2 h before administration of EFV. The microdialysis probe was perfused with a solution containing

 doi:10.2217/NNM.12.104

147 mM NaCl, 2.4 mM $CaCl_2$ and 4 mM KCl (pH 7.3), employing a perfusion pump (flow = 1 µl/min). Different EFV-loaded specimens (20 and 30 mg/ml, 40 µl) were administered iv. (tail vein) or in. employing Hamilton syringes (100 µl) with standard (iv.) or true short bevel (in.). After administration, microdialysis samples (15 µl) were collected every 15 min (over 4 h) to quantify the EFV in the CNS. In parallel, blood samples (50 µl) were obtained from the tail vein at 5, 15, 30, 60, 90 and 120 min [45]. It is worth noting that the maximum in. administration volume in rats was approximately 20 µl per nostril. The *in vitro* recovery of the microdialysis probe was determined after each experiment.

Sample analysis

Blood samples (tail vein, ~70–100 µl) were collected in heparin solution (25 U/ml, 10 µl) and centrifuged (10,000 rpm, 10 min, 4°C) to isolate plasma. Plasma (10 µl) was deproteinized by adding acetonitrile (20 µl, 10 s of hand shaking followed by 8 min centrifugation at 9000 rpm and 4°C). Subsequently, the drug concentration was determined by liquid chromatography (HPLC, see below). Dialysates (microdialysis) were analyzed without any pretreatment; deproteinization was not required. The EFV concentration in the different samples was measured by HPLC, adapting a previously reported technique [61]. The system was comprised of a Phenomenex Luna 5 µm, C18, 150 mm × 4.60 mm column (Phenomenex, CA, USA) with a UV detector (248 nm, UVIS 204, Linear Instruments, NV, USA) [45,46]. The mobile phase (distilled water:acetonitrile:triethylamine, 60:40:0.2, pH 3) was pumped at a flow rate of 1.4 ml/min. The analytical method for quantification was linear in the 20–5000 ng/ml range.

PK analysis

Concentrations of EFV in hypothalamic dialysates were corrected by the *in vitro* recovery of the concentric microdialysis probe (0.08 ± 0.03). Noncompartmental analysis of EFV plasma concentrations was performed using the TOPFIT program (version 2.0, Dr Karl Thomae Gmbh, Schering AG, Gödecke AG, Freiburg, Germany), which uses a cyclic three-stage optimization routine (1D direct search; vectorial direct search/Hooke-Jeeves modified; Gauss-Newton/Marquadt modified). The relative exposure index was calculated by taking the ratio between the area under the curve (AUC) between 0 and 2 h in CNS and plasma, AUC_{p0-2h} and $AUC_{CNS0-2h}$, respectively.

Statistical analysis

PK parameters were log transformed for statistical analysis to reduce heterogeneity of the variance and further compared by one-way analysis of variance and the Bonferroni test, as a *post-hoc* test. Statistical analysis was performed using GraphPad Prism version 5.02 for Windows (GraphPad Software, CA, USA). Statistical significance was defined as $p < 0.05$.

Integrity of the BBB

The integrity of the BBB was evaluated by means of the Evans blue (EB) dye (Sigma) extravasation method [62]. A total of 5 mins after the administration of EFV-loaded pF127–20 micelles (iv.), EB solution (2%, 1 ml/kg, in 0.9% NaCl) was administered iv. Animals were perfused with 4 ml of heparinized saline solution and euthanized 30 min after the EB injection by decapitation. Brains were subsequently harvested, freeze-dried and weighed. To quantify the amount of EB, dissected tissues were immersed in a volume of dimethylformamide equal to six-times the weight of the tissue [62]. Whole brains were homogenized and incubated at 50°C for 24 h. Subsequently, each sample was centrifuged for 30 min at 7000 rpm to isolate the dye solution (supernatant) and dye concentrations were determined by UV-Visible spectrophotometry (Shimadzu UV-Visible Recording Spectrophotometer UV-260, Kyoto, Japan) at a wavelength of 633 nm, using a standard plot of the dye in dimethylformamide (concentration range 6–30 µg/ml, $R^2 = 0.9994$). A positive control of augmented BBB permeability was obtained by administering (iv.) a hyperosmolar mannitol solution (1.6 M in 0.9% NaCl, 4 ml), while a blank was obtained by administering the dye (iv.) directly without any previous treatment. Results are expressed as the mean ± standard deviation (n = 3).

Results & discussion

With the aim to increase the bioavailability of EFV in the CNS, the present study investigated for the first time the performance of nanoscopic drug-loaded polymeric micelles administered intranasally and compared the PKs with that of the same systems upon iv. administration. To investigate the effect of micellar size, micellar composition and drug payload, we employed simple polymeric micelles made of a highly hydrophilic copolymer, poloxamer F127, and mixed polymeric micelles containing 75% of T904 (a medium hydrophobic poloxamine) and 25% of F127. T904 improves the encapsulation

capacity of the micelles, while F127 confers greater physical stability to the drug-loaded systems [48].

The EFV encapsulation capacity of a broad spectrum of PEO–PPO copolymers displaying different molecular weight, hydrophilic–lipophilic balance and architecture (linear and branched) was previously assessed employing different copolymer concentrations [45–48] and the incorporation of the drug into the micellar core was confirmed by ^{1}H-NMR [48]. All of the EFV-loaded micelles displayed sizes in the nanoscopic level. For example, 10% pF127 micelles resulted in an encapsulation capacity of 21.5 mg/ml, representing an aqueous solubility increase of 5365-times [45]. T904 micelles were more efficient, with 10% micelles encapsulating 29.5 mg/ml [47]. Mixed micelles were developed to capitalize on the better physical stability of EFV-loaded pF127 micelles and the greater encapsulation capacity of T904 micelles [48]. In addition, these copolymers showed a synergistic effect, 10% F127:T904 (25:75) mixed micelles encapsulating up to 34 mg/ml of EFV. In this framework, pF127–20 and F127:T904–30 systems contained EFV payloads that were slightly below their corresponding maximum encapsulation capacity. Conversely, F127:T904–20 micelles were not saturated with the drug.

Micellar size, size distribution & physical stability

EFV-loaded pure and mixed polymeric micelles are stable at 25 and 37°C for prolonged periods of time [45–48]. However, dilution in body fluids (e.g., blood) and adsorption of plasma proteins after iv. administration could affect the physical stability and modify the size and the size distribution of the micelles. To assess the behavior of the micelles in the biological environment, EFV-loaded micelles were primarily diluted in PBS with 1 and 3% bovine serum albumin (1/20), stored at 37°C and characterized by dynamic light scattering over 24 h. This BSA concentration was in the range of the physiological concentration, usually between 3.5 and 5.0 g/dl, and it was previously employed to assess the physical stability of polymeric micelles [63]. Previous works indicated that micelles could remain relatively unchanged for at least 25 h (with a steady size growth afterwards) or conversely, they could undergo a sharp and fast size increase due to a protein-mediated clustering [64,65]. This behavior depended on the hydrophilicity of the micellar corona and its ability to interact with BSA. pF127–20 and F127:T904–20 micelles displayed relatively small initial sizes of 23.0 and 13.5 nm, respectively, at 37°C (Table 1) and their morphology was spherical, as exemplified for pF127:T904–20 in Figure 1. The former were saturated with the drug, while the latter were not. Conversely, the encapsulation of a greater EFV payload led to the enlargement of the mixed micelles from 13.5 nm in F127:T904–20 to 247.3 nm in F127:T904–30. Sizes before dilution were more relevant for the in. administration route because in this case, samples were not expected to undergo dilution in the bloodstream before entering the CNS.

In general, dilution of systems containing an EFV payload of 20 mg/ml in PBS (pH 7.4) and 1% BSA led to a slight growth of the size and size distribution. For example, pF127–20 micelles grew from 22.8 to 27–30 nm and F127:T904–20 from 13.5 to 18–23 nm. In addition, F127:T904–20 diluted in PBS displayed a large size fraction of several hundreds of nanometers that increased in intensity over time. This phenomenon was not observed in 1% BSA, suggesting that the sharp size growth in PBS probably stemmed from a salting-out effect. Contrary to this, F127:T904–30 micelles showed a sharp size decrease from 247.0 to 110–120 nm; the dilution in PBS and 1% BSA having a similar effect. Since the corona of PEO–PPO micelles is made of PEO, it probably prevented the adsorption of proteins such as BSA and changes in the aggregation pattern could be exclusively ascribed to dilution [65,66]. When a greater BSA concentration was used, pF127–20 showed a bimodal size pattern. The smaller aggregates (10–11 nm) would correspond to F127 micelles of unchanged sized, while the larger ones (38–45 nm) correspond to enlarged micelles. These systems also showed a similar behavior at 25°C [45]. On the other hand, the hindrance of F127 self-aggregation by greater BSA concentrations (3%) could not be ruled out because the micellization of highly hydrophilic PEO–PPO copolymers is intrinsically incomplete [32]. Dilution of F127:T904–20 in 3% BSA maintained the original monomodal pattern with a moderate size decrease from 18 to 10 nm, confirming that even if it was not adsorbed on the PEG corona, the protein could affect the copolymer self-aggregation process. When diluted in a greater concentration of BAS, F127:T904–30 remained unaltered. In summary, the size order in all the investigated conditions *in vitro* was F127:T904–30 >>> pF127 > F127:T904–20. It is worth stressing that the size of the micelles always remained smaller than 120 nm and in

 doi:10.2217/NNM.12.104

Table 1. Hydrodynamic diameter and size distribution of efavirenz-loaded micelles (10%) over 24 h, at 37°C.

Medium	Dilution	Time (h)	pF127–20				PDI (±SD)	F127:T904–20				PDI (±SD)	F127:T904–30		PDI (±SD)
			Peak 1		*Peak 2*			*Peak 1*		*Peak 2*			*Peak 1*		
			D_h (nm) (±SD)	*%*	*D_h (nm) (±SD)*	*%*		*D_h (nm) (±SD)*	*%*	*D_h (nm) (±SD)*	*%*		*D_h (nm) (±SD)*	*%*	
PBS pH 7.4	-	0	22.8 (0.3)	100.0	-	-	0.299 (0.008)	13.5 (0.1)	100.0	-	-	0.223 (0.012)	247.3 (7.3)	100.0	0.222 (0.012)
PBS pH 7.4	1/20	2	27.1 (0.4)	100.0	-	-	0.041 (0.008)	23.6 (0.5)	100.0	-	-	0.228 (0.008)	107.8 (1.2)	100.0	0.085 (0.011)
		4	27.8 (0.6)	100.0	-	-	0.052 (0.008)	23.0 (0.9)	78.40	311.3 (65.5)	21.6	0.343 (0.007)	110.9 (0.5)	100.0	0.090 (0.001)
		8	28.7 (0.3)	100.0	-	-	0.079 (0.005)	22.1 (0.3)	68.10	236.7 (16.0)	31.9	0.414 (0.026)	115.7 (2.5)	100.0	0.133 (0.004)
		24	30.0 (0.5)	100.0	-	-	0.115 (0.007)	21.4 (0.1)	51.50	301.8 (6.9)	48.5	0.608 (0.083)	120.2 (0.4)	100.0	0.123 (0.008)
BSA 1%		2	27.6 (0.4)	100.0	-	-	0.371 (0.056)	18.6 (1.0)	100.0	-	-	0.249 (0.004)	108.6 (7.1)	100.0	0.259 (0.017)
		4	28.4 (0.8)	100.0	-	-	0.326 (0.006)	18.0 (0.6)	100.0	-	-	0.228 (0.007)	109.5 (2.3)	100.0	0.240 (0.003)
		8	28.8 (0.6)	100.0	-	-	0.351 (0.001)	18.3 (0.6)	100.0	-	-	0.218 (0.004)	115.6 (2.1)	100.0	0.227 (0.006)
		24	28.2 (0.5)	100.0	-	-	0.380 (0.052)	18.6 (0.7)	100.0	-	-	0.226 (0.001)	113.1 (6.4)	100.0	0.232 (0.007)
BSA 3%		2	10.9 (0.2)	58.0	43.6 (1.1)	42.0	0.310 (0.014)	9.8 (0.1)	100.0	-	-	0.235 (0.004)	110.4 (0.3)	100.0	0.228 (0.011)
		4	11.0 (0.0)	57.8	44.5 (1.2)	42.2	0.327 (0.001)	10.0 (0.1)	100.0	-	-	0.247 (0.008)	109.1 (1.7)	100.0	0.228 (0.003)
		8	10.1 (0.8)	51.9	41.1 (4.2)	48.1	0.335 (0.002)	10.1 (0.1)	100.0	-	-	0.213 (0.001)	111.1(1.3)	100.0	0.219 (0.001)
		24	10.3 (0.1)	52.1	38.4 (0.6)	47.9	0.345 (0.004)	10.2 (0.1)	100.0	-	-	0.222 (0.007)	111.6 (0.8)	100.0	0.206 (0.011)

BSA: Bovine serum albumin; D_h: Hydrodynamic diameter; PBS: Phosphate-buffered saline; PDI: Polydispersity index; SD: Standard deviation.

doi:10.2217/NNM.12.104

future science group fsg

the optimal size range for CNS targeting by in. administration [52].

PK studies

Owing to the limited preclinical experience with in. administration, the maximum volume that can be administered to rats has not been well established. Based on data of the liquid instillation in mice [67] and aiming to maximize the amount of EFV that enters the nose-to-brain route, we systematically administered a drug-fixed dose of 0.8 or 1.2 mg (encapsulated in 40 µl of 10% micelles; 20 µl/nostril). Then, drug concentrations in plasma and CNS were followed up. As opposed to water-soluble ARVs such as zidovudine and didanosine [54,55] that can be administered intranasally as concentrated solutions, EFV is poorly water-soluble and it can be solubilized directly in water to an extent that would enable the administration of a sufficiently high dose and the detection in body fluids. Conversely, EFV is soluble in some organic solvents (e.g., alcohols) that are unsuitable for intranasal formulations. Moreover, there is evidence that drugs encapsulated within polymeric nanocarriers reach the CNS after intranasal administration more effectively than the soluble form. In this framework, only EFV-loaded micelles were assessed.

To minimize the number of animals employed in the study, EFV concentrations in the CNS were monitored by a microdialysis technique (Figure 2) that employs a semipermeable micron-sized membrane (external diameter of 190 µm) (Figure 3) inserted into the anterior hypothalamus by means of stereotaxy [68]. After the insertion of the canula, the device was equilibrated for 2 h before administration of EFV to ensure the complete sealing of the BBB and to prevent the formulation of any artifact derived from the increased permeability of a damaged BBB [69]. A 2 h end-point was selected owing to ethical concerns and to minimize animal suffering.

The iv. administration of pF127–20 and F127:T904–20 resulted in C_{max} values in plasma of 1.792 and 1.632 µg/ml, regardless of the difference in micellar size and composition (Figure 4, Table 2). $AUC_{p0–2h}$ followed a similar trend with values of 1.465 and 1.487 µg/ml/h. As expected, the increase of the EFV payload from 20 to 30 mg/ml (and consequently of the EFV dose from 0.8 to 1.2 mg) led to a clear increase of C_{max} from 1.632 to 2.403 µg/ml; a 50% greater dose resulted in a 60–62% increase of the $AUC_{p0–2h}$. In addition, different micelles resulted only in slight changes of the biological half-life ($t_{1/2}$); $t_{1/2}$ were 1.625, 1.947 and 1.575 h for pF127–20, F127:T904–20 and F127:T904–30, respectively (Table 2). After the oral administration of drug-loaded micelles, the drug is expected to be absorbed by the intestinal epithelium deprived of the nanocarrier (non-encapsulated), though the internalization of micelles by fluid-phase pinocytosis could not be ruled out [70]. In this context, the clearance from plasma was not majorly modified with respect to

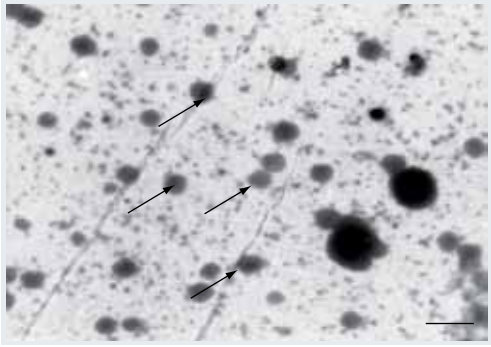

Figure 1. Transmission electron micrograph of efavirenz-loaded pF127:T904–20 micelles. The characteristic spherical morphology of PEO–PPO micelles was apparent (indicated with arrows). Scale bar = 100 nm.

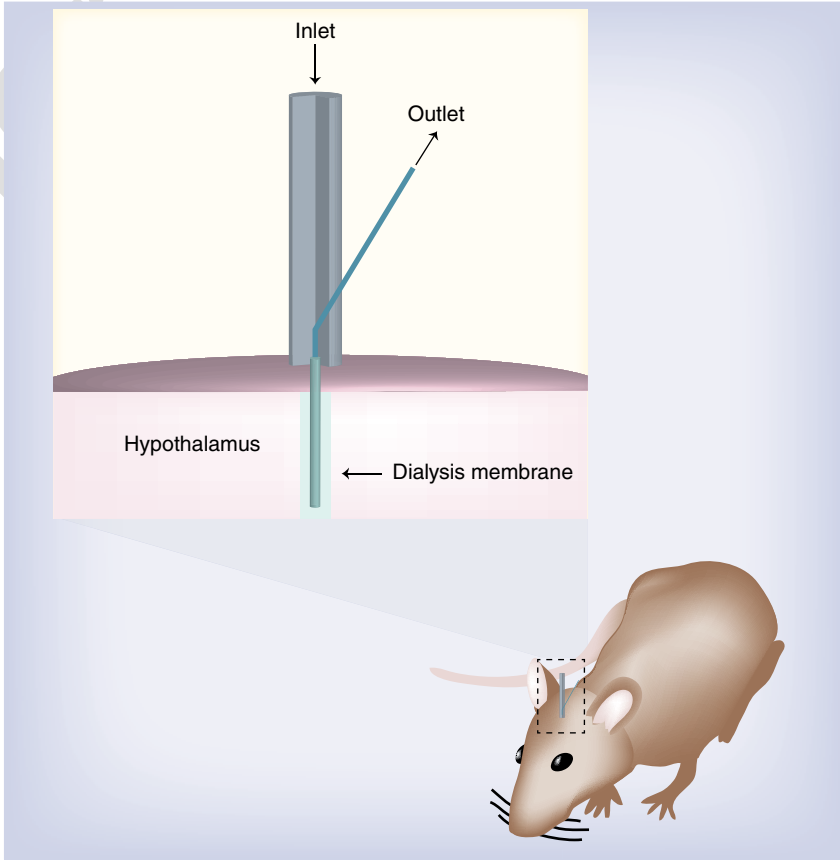

Figure 2. Microdialysis setup for the monitoring of efavirenz concentration in the CNS after the intravenous and intranasal administration of efavirenz-loaded polymeric micelles.

doi:10.2217/NNM.12.104

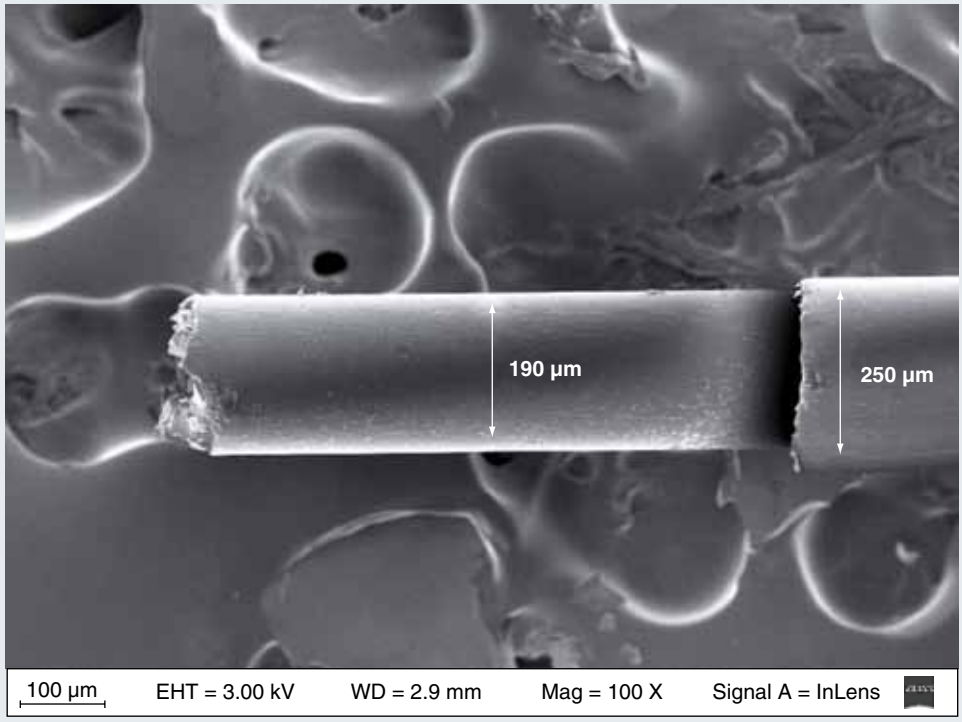

Figure 3. Scanning electron microphotograph of the microdialysis probe employed to monitor efavirenz concentrations in the CNS.

the same drug administered in any another pharmaceutical form (e.g. suspension). Conversely, the parenteral administration (e.g., iv.) implies that all the encapsulated drug reaches the systemic circulation within the nanocarrier. Thus, we expected changes in the drug elimination rate owing to differences in micellar size and composition. However, $t_{1/2}$ values in plasma did not change substantially among the different micelles. After iv. administration, EFV was detected in the brain. However, concentrations were substantially smaller than those found in plasma. For example, C'_{max} and $AUC_{CNS0-2h}$ values ranged between 0.495 and 0.820 µg/ml and 0.530 and 0.978 µg/ml/h, respectively (TABLE 2). These results suggested that EFV entered the CNS only upon redistribution from the bloodstream. Interestingly, two systems containing identical EFV payloads but different micellar size and composition, namely pF127–20 and F127:T904–20, resulted in very different CNS profiles. The smaller the size, the greater the CNS bioavailability observed. Although not reaching statistical significance ($p = 0.09$), $AUC_{CNS0-2h}$ values were 0.530 and 0.762 µg/ml/h for pF127–20 and F127:T904–20, respectively. A priori, the difference in size appears to be small to explain an increase of the bioavailability of approximately 50%.

Increasing the drug payload from 20 mg/ml in F127:T904–20 to 30 mg/ml in F127:T904–30 (two nanocarriers of identical copolymer composition and significantly different size) and the dose from 0.8 to 1.2 mg led to a less pronounced increase of 29% in the $AUC_{CNS0-2h}$. When the performance of pF127–20 was compared with that of F127:T904–30, a 50% greater dose represented a 65 and 85% increase of C'_{max} and $AUC_{CNS0-2h}$, respectively. It is important to note that the size of pF127–20 and F127:T904–20 was similar. These findings strongly suggested that the size was not

Figure 4. Plasma and brain efavirenz concentrations after the administration of the different efavirenz-loaded micelles by the intravenous and intranasal routes (n = 6).

Table 2. Pharmacokinetic parameters of the different efavirenz samples (40 µl) administered by the intravenous and intranasal route (n = 6).

Route	Parameters		EFV (20 mg/ml)†		EFV (30 mg/ml)†
			pF127–20	*F127:T904–20*	*F127:T904–30*
Intravenous	CNS	C'_{max} (µg/ml)	0.495 (0.185)	0.697 (0.158)	0.820 (0.261)
		t_{max} (h)	0.563 (0.119)	0.583 (0.129)	0.625 (0.072)
		$AUC_{CNS0-2h}$ (µg/ml/h)	0.530 (0.100)	0.762 (0.132)	0.978 (0.253)
		$t_{1/2}$ (h)	1.018 (0.299)	1.157 (0.165)	0.836 (0.076)
	Plasma	C_{max} (µg/ml)	1.792 (0.389)	1.632 (0.229)	2.403‡ (0.091)
		t_{max} (h)	-	-	-
		AUC_{p0-2h} (µg/ml/h)	1.465 (0.235)	1.487 (0.276)	2.378‡§ (0.094)
		$t_{1/2}$ (h)	1.625 (0.142)	1.947 (0.328)	1.575 (0.229)
	AUC_{rel}		0.374 (0.056)	0.540 (0.062)	0.404 (0.089)
Intranasal	CNS	C'_{max} (µg/ml)	1.400 (0.343)	1.955 (0.336)	3.102 (0.831)
		t_{max} (h)	0.500 (0.102)	0.417 (0.066)	0.583 (0.129)
		$AUC_{CNS0-2h}$ (µg/ml/h)	1.703 (0.422)	2.465 (0.493)	3.638 (0.531)
		$t_{1/2}$ (h)	0.931 (0.231)	1.480 (0.207)	0.723 (0.105)
	Plasma	C_{max} (µg/ml)	1.319 (0.366)	0.743 (0.219)	1.672‡§ (0.546)
		t_{max} (h)	0.280 (0.098)	0.193 (0.044)	0.402 (0.174)
		AUC_{p0-2h} (µg/ml/h)	1.328 (0.330)	0.908 (0.202)	1.815† (0.275)
		$t_{1/2}$ (h)	1.456 (0.368)	2.063 (0.565)	1.735 (0.777)
	AUC_{rel}		1.305¶ (0.334)	2.931§¶ (0.487)	2.166¶ (0.512)

CNS values were determined between 0 and 2 h.
AUC_{rel} was calculated as the ratio between AUC_{CNS} and AUC_p.
†mean(± SEM)
‡p < 0.05 vs F127:T904–20.
§p < 0.05 vs pF127.
¶p < 0.05 vs intravenous administration.
AUC_{rel}: Area under the curve relative exposure index; C'_{max}: ??? ; EFV: Efavirenz; SEM: Standard error of mean;

the only parameter governing drug absorption from plasma into the CNS.

EFV display a nonlinear oral PKs upon oral and iv. administration [71] and a relatively long half-life [37]. This behavior could stem from two mechanisms: saturation of the metabolism and prolongation of the absorption in the gut. Both mechanisms could explain the exponential bioavailability increase after per orem administration, while in the case of iv., the only possible pathway is the former. The present work investigated the feasibility of this strategy to improve the bioavailability of the drug in CNS. Thus, extensively assessing the effect of the dose on the EFV PKs was beyond the scope of this article. Having expressed this, when the dose was increased from 0.8 to 1.2 mg, the effect on the bioavailability was strongly associated with the properties of the nanocarrier (e.g., size and composition).

To compare the relative brain exposure for different specimens after both administration routes, a relative exposure index (AUC_{rel}) was calculated by taking the ratio between $AUC_{CNS0-2h}$ and AUC_{p0-2h}. After iv. administration, values were 0.374 and 0.540 for pF127–20 and F127:T904–20, respectively, confirming that the systemic exposure was greater than in the brain. Although the difference was not statistically different ($p = 0.058$), these results suggested that EFV encapsulated within the more hydrophobic T904-containing micelles surpassed the BBB more effectively (Table 2). Interestingly, F127:T904–30 led to higher absolute CNS and plasma concentrations, though to a smaller AUC_{rel} value of 0.404. Two mechanisms could explain this phenomenon: the saturation of the drug passage from plasma to CNS and the more constrained passage across the BBB of drugs encapsulated in remarkably larger

doi:10.2217/NNM.12.104

Figure 5. Rat brains excised after the administration of 2% Evans blue (intravenous, 1 ml/kg) water solution. (A) Evans blue (EB) after no treatment (control), **(B)** EB after treatment with mannitol 1.6 M (4 ml, intravenous) and **(C)** EB after treatment with efavirenz-loaded pF127 micelles (40 µl, intravenous). The lag time between both administrations was 5 min.

micelles. Again, the size difference between both micelles containing 20 mg/ml drug seems to be very small to explain the sharp increase shown by F127:T904–20 with respect to pF127–20.

Previous investigations showed greater CNS bioavailability upon iv. administration of drugs encapsulated within polymeric NPs coated with poloxamer F68, a very hydrophilic PEO–PPO–PEO triblock with negligible inhibitory activity of ABCs [72]. The mechanism relied on the surface adsorption of apolipoproteins, such as apolipoprotein A-I (Apo A-I) and the selective interaction of the nanocarrier with the scavenger receptor B Class I, expressed in the membrane of brain endothelial cells [73]. Since F68, F127 and T904 display terminal blocks of identical chemical nature, a similar adsoprtion pattern of Apo A-I could be anticipated. Thus, a different BBB uptake based on this mechanism for the different micelles studied could be most likely neglected.

The inhibition of the functional activity of P-glycoprotein and BCRP by very low concentrations of T904 was recently demonstrated in different intestinal and hepatic cell lines [74,75]. The authors of this study have also tracked the inhibition of BCRP down to the nucleus, where a clear decrease of the mRNA encoding for these two pumps was confirmed by RT-PCR [76]; BCRP is one of the main ABCs in the BBB and EFV is a substrate of this pump in the intestines and brains of rats [40,41]. Accordingly, *in vivo* data would suggest that the T904 present in F127:T904–20 inhibited the activity of BCRP pumps and enhanced the EFV concentration in the CNS with respect to pF127–20, a system with identical drug payload and similar size, though without T904. Subsequently, when both nanocarriers contained T904, the size played a more relevant role and the smaller F127:T904–20 micelles counterbalanced the dose increase in the larger F127:T904–30 micelles.

The intranasal administration of different drug-loaded micelles led to a sharp three- to four-fold increase of C'_{max} and $AUC_{CNS0-2h}$ (Figure 4); values ranged between 1.400–3.102 µg/ml and 1.703–3.638 µg/ml/h, respectively. Conversely, a sharp decrease of the systemic exposure as estimated by the drug concentration in plasma was observed. For example, C_{max} values decreased from 1.792, 1.632 and 2.403 to 1.319, 0.743 and 1.672 µg/ml, for pF127–20, F127:T904–20 and F127:T904–30, respectively. These data suggested that once released into the CNS, the drug was redistributed into the systemic circulation.

It is also noteworthy that regardless of the relatively small size difference between pF127–20 and F127:T904–20 micelles, the latter led to a substantial (though not statistically significant) increase of $AUC_{CNS0-2h}$ with respect to the former; the values being 1.703 and 2.465 µg/ml/h, respectively. The opposite was true for plasma concentrations with AUC_{p0-2h} of 1.328 and 0.908 µg/ml/h for the pure and mixed micelles. Consequently, the

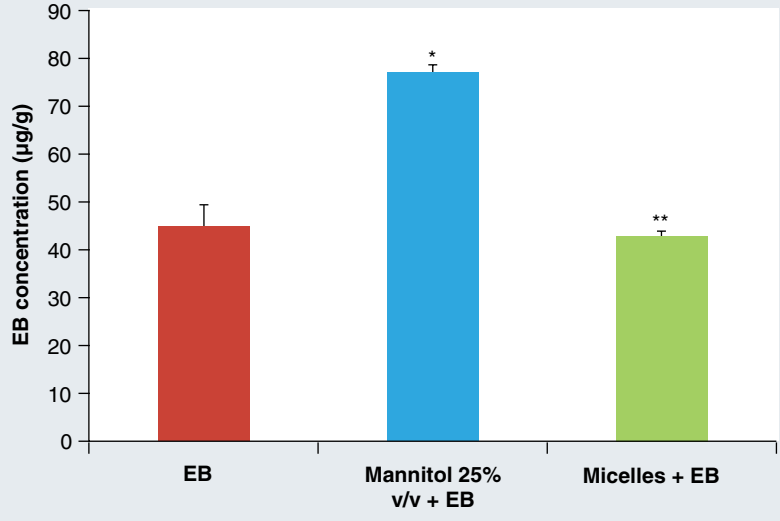

Figure 6. Evans blue concentration in rat brains (µg/g of dry brain) excised after the administration of 2% Evans blue solution (intravenous, 1 ml/kg) water solution after no treatment (control), mannitol 1.6M (4 ml, intravenous) and pF127–20 micelles (40 µL, intravenous) (n = 3). The lag time between both administrations was 5 min.
*Difference is statistically significant with respect to the control ($p < 0.05$).
**Difference is not statistically significant with respect to the control ($p < 0.05$).
EB: Evans blue.

AUC_{rel} of F127:T904–20 after intranasal administration was twofold greater than that of pF127–20. As mentioned above, micelles do not undergo substantial dilution upon intranasal administration. Remarkably, AUC_{rel} values increased from 0.374–0.540 (iv.) to 1.305–2.931 (in.), representing up to a 5.4-fold increase of the relative CNS exposure with respect to plasma (Table 2). On the other hand, $t_{1/2}$ values after intransal administration were not significantly different than those after intravenous administration (Table 2).

The increase of the relative CNS/plasma exposure depends on the properties of the nanocarriers (e.g., size and composition) as well as the drug, thus comparing different systems is complex. Having said this, EFV-loaded micelles showed improvement extents that were comparable to those in the literature [53,55]. On the other hand, due to the self-assembly nature of these systems, the release could not be extended.

Although the mechanisms for nose-to-brain transport are not fully understood, there is sufficient evidence that olfactory and trigeminal nerves are involved in the process and the size of the NPs plays a key role [50,51]. However, the upper size limit to enable nose-to-brain transport is still controversial. While some authors initially established it at 100 nm [50], Kanazawa *et al.* showed no difference in the brain uptake of coumarin-loaded NPs between sizes of 100–300 and 200–600 nm [52]. Conversely, when the size increased from 100 to 600 nm, a significant decrease in uptake was observed. In addition, nanocarriers smaller than 100 nm have shown facilitated mucosal and transcellular transport via endocytic pathways. In this framework, smaller structures appeared more optimal for intranasal delivery. Regardless of the great size difference between F127:T904–20 and F127:T904–30, a 50% increase of the EFV dose increased both C_{max} and AUC_{0-2h} to a similar extent. These findings indicated that the size was not the main parameter to be considered, especially when micelles had different compositions. In this context, a comprehensive evaluation of each delivery system needs to be addressed.

The inhibition of BCRP is also a feasible mechanism to explain differences in the bioavailability after intranasal administration [50] because ABCs are also present in the olfactory epithelium. The remarkable bioavailability difference found between pF127–20 and F127:T904–20 micelles constitutes further evidence that the micellar composition governed the PKs of EFV and that T904 could be playing a dual role of nanocarrier and ABC inhibitor.

Integrity of the BBB

Although microdialysis is a well-established methodology to monitor drug concentrations in the CNS, the insertion of the probe transiently alters the integrity of the BBB. The equilibration time was supposed to ensure the complete closure of the injured BBB. Moreover, PEO–PPO copolymers could also alter the permeability of this barrier.

In this work, we assayed both qualitatively and quantitatively the effect of these amphiphiles on the permeability of the BBB after iv. administration by means of the EB staining technique. EB binds to plasma albumin and reveals the extravasation of this protein due to the increased permeability of the BBB associated with transient or permanent damage. The mere qualitative analysis is subjective because only the cortical surface of the brain stains [77]. Moreover, previous studies demonstrated that a small percentage of EB (~5%) could reach the brain even in the presence of an intact BBB [62]. To make this analysis more robust, brains were harvested, homogenized, freeze-dried and the total amount of dye per weight quantified by UV-Vis spectrophotometry. Since this EB–protein association is unfeasible when the system is administered intranasally, we focused on intravenous administration.

A negative control (microdialysis probe + iv. EB) did not show any coloration detectable by the naked eye (Figure 5A). In addition, the EB concentration was 44.9 µg/g; this concentration representing 5.6% of the administered EB (Figure 5). This result was in full agreement with the literature [63] and indicated that the 2 h equilibration time ensured complete sealing of the BBB. Contrary to this, a positive control (microdialysis probe + iv. mannitol + iv. EB) resulted in the typical blue coloration of the brain surface (Figure 5B), the EB concentration being 77 µg/g (9.6% of the injected dose) (Figure 6); the difference with respect to a negative control was statistically significant ($p < 0.05$). Mannitol is a known hyperosmotic agent that transiently increases the permeability of the BBB. Similar to the control, EFV-loaded pF127–20 micelles did not stain the brain (Figure 5C) and showed a concentration of 43 µg/g (5.3% of the injected dose) (Figure 6). There was no significant difference with respect to a negative control ($p < 0.05$). These findings would confirm that this copolymer did not alter the permeability of the BBB.

doi:10.2217/NNM.12.104

Conclusion

In this work, we reported for the first time the intranasal administration of ARV-loaded polymeric micelles as a strategy to improve the bioavailability of these drugs in the CNS. In contraposition with previous works, our findings suggested that size is not the main parameter governing the absorption from the nasal mucosa and highlighted the contribution of tnanocarrier composition. This aspect is especially relevant owing to the inhibition of BCRP pumps involved in EFV removal from the CNS by T904. The nanoscopic nature of these EFV-loaded micelles could play a fundamental role in cell internalization mechanisms that are relevant to the activity of the encapsulated drug in HIV-infected cells. Since PEO–PPO micelles display a PEGylated surface, uptake by phagocytic cells would probably be curtailed. In fact, this feature prolongs the circulation time of PEO–PPO micelles in the bloodstream. In this context, studying the interaction between these drug-loaded micelles and a representative HIV-infected cell type *in vitro* (e.g., macrophages) would shed light on additional internalization mechanisms that could govern the performance of the ARV. The main goal of the present study was to explore the capacity of the intranasal administration of EFV-loaded micelles to surpass the BBB and to increase the drug bioavailability with respect to a more conventional route, such as intravenous administration. Future studies will need to address the nanocarrier–cell interaction and more importantly the effectiveness of this strategy in a preclinical model of HIV-infected CNS. Finally, EFV-loaded micelles did not display a sustained release profile owing to their self-assembly nature. Thus, a different type of polymeric nanocarrier should be engineered to extend the release and eventually reduce the administration frequency.

Future perspective

Regardless of the advantages of this minimally invasive administration route, the potential to reach the CNS remains unexplored and uncapitalized. Studies investigating the most appropriate positions [78] and the development of devices that enable accurate dosing [79] may further contribute to consolidate our understanding of the key parameters of this administration route and pave the way to clinical implementation.

Acknowledgements

The authors thank Carlos Taira for technical assistance in brain harvesting.

Financial & competing interests disclosure

The authors thank the University of Buenos Aires (Grants UBACyT 20020090200016 and 20020100300088) and the CONICET (Grant PIP0220) for financial support. The authors have no other relevant affiliations or financial involvement with any organization or entity with a financial interest in or financial conflict with the subject matter or materials discussed in the manuscript apart from those disclosed.

No writing assistance was utilized in the production of this manuscript.

Ethical conduct of research

Animal experiments were in line with the 'Principles of laboratory animal care' (NIH publication No. 85–3, revised 1985) and local regulations. The authors state that they have obtained appropriate institutional review board approval or have followed the principles outlined in the Declaration of Helsinki for all human or animal experimental investigations. In addition, for investigations involving human subjects, informed consent has been obtained from the participants involved.

Executive summary

Intravenous pharmacokinetics

- After intravenous administration, efavirenz was also detected in brain. However, concentrations were substantially smaller than those found in plasma.

Effect of micellar composition on intravenous pharmacokinetics

- Mixed micelles containing T904 increased the bioavailability in the CNS to a greater extent than pure micelles without T904, indicating that the drug encapsulated in these micelles surpassed the blood–brain barrier more effectively.

Effect of micellar size on intravenous pharmacokinetics

- Micellar size played a key role only when micelles displayed an identical composition; the smaller the size, the greater the bioavailability in the CNS. Otherwise, the composition was more relevant.

Intranasal pharmacokinetics

- After intranasal administration, efavirenz concentrations in brain markedly increased, representing a 5.4-fold increase of relative CNS exposure with respect to plasma.

Effect of poloxamine T904 on the bioavailability

- The remarkable bioavailability difference found between micelles with and without T904 strongly suggested that T904 would play a dual role of nanocarrier and ATP-binding cassette inhibitor.

References

Papers of special note have been highlighted as:
▪ of interest
▪▪ of considerable interest

1 Gazzard BG, Jones RS. From death to life: two decades of progress in HIV therapy. In: *HIV/AIDS in Europe: Moving from Death Sentence to Chronic Disease Management*. Matic S, Lazarus JV, Donoghoe MC (Eds). World Health Organization Regional Office for Europe Publications, Copenhagen Ø: World Health Organization Publications, 101–117 (2006).

2 De Clercq E. Antiretroviral drugs. *Curr. Opin. Pharmacol.* 10, 507–515 (2010).

3 Romanelli F, Hoven AD. Use of virostatics as a means of targeting human immunodeficiency virus infection. *Curr. Pharm. Des.* 12, 1121–1117 (2006).

4 Park S, Sinko P. P-glycoprotein and multidrug resistance-associated proteins limit the brain uptake of saquinavir in mice. *J. Pharmacol. Exp. Ther.* 312, 1249–1256 (2005).

▪ **Pioneering study showing the involvement of efflux pumps of the ATP-binding cassette superfamily in the limited passage of antiretrovirals through the blood–brain barrier.**

5 Geeraert L, Kraus G, Pomerantz RJ. Hide-and-seek: the challenge of viral persistence in HIV infection. *Ann. Rev. Med.* 59, 487–501 (2008).

6 Padowski JM, Pollack GM. Examination of the ability of the nasal administration route to confer a brain exposure advantage for three chemical inhibitors of P-glycoprotein. *J. Pharm. Sci.* 99, 3226–3233 (2010).

7 Csajka C, Marzollini C, Fattinger K *et al.* Population pharmacokinetics and effects of efavirenz in patients with human immunodeficiency virus infection. *Clin. Pharm. Ther.* 73, 20–30 (2003).

8 Aarnoutse R, Schapiro JM, Bouchr CAB, Hkster YA, Burger DM. Therapeutic drug monitoring. *Drugs* 63, 741–753 (2003).

9 Aungst BJ. P-glycoprotein, secretory transport, and other barriers to the oral delivery of anti-HIV drugs. *Adv. Drug Del. Rev.* 39, 105–116 (1999).

10 Balimane PV, Sinko PJ. Involvement of multiple transporters in the oral absorption of nucleoside analogues. *Adv. Drug Del. Rev.* 39, 183–209 (1999).

11 Shaik N, Giri N, Pan G, Elmquist WF. P-glycoprotein-mediated active efflux of the anti-HIV1 nucleoside abacavir limits cellular accumulation and brain distribution. *Drug Metabol. Dispos.* 35, 2076–2085 (2007).

▪ **Study showing the involvement of efflux pumps of the ATP-binding cassette superfamily in the limited passage of antiretrovirals through the blood–brain barrier.**

12 Ronaldson PT, Persidsky Y, Bendayan R. Regulation of ABC membrane transporters in glial cells: relevance to the pharmacotherapy of brain HIV-1 infection. *Glia* 56, 1711–1735 (2008).

▪▪ **Update on the role played by ATP-binding cassette pumps in the progress of HIV infection in the CNS.**

13 Vivithanaporn P, Gill MJ, Power C. Impact of current antiretroviral therapies on neuroAIDS. *Expert Rev. Anti Infect. Ther.* 9, 371–374 (2011).

14 Nath A, Sacktor N. Influence of highly active antiretroviral therapy on persistence of HIV in the central nervous system. *Curr. Opin. Neurol.* 19, 358–361 (2006).

15 Crews L, Patrick C, Achim CL, Everall IP, Masliah E. Molecular pathology of neuro-AIDS (CNS-HIV). *Int. J. Mol. Sci.* 10, 1045–1063 (2009).

16 Dash PK, Gorantla S, Gendelman HE *et al.* Loss of neuronal integrity during progressive HIV-1 infection of humanized mice. *J. Neurosci.* 31, 3148–3157 (2011).

17 Grovit-Ferbas K, Harris-White ME. Thinking about HIV: the intersection of virus, neuroinflammation and cognitive dysfunction. *Immunol. Res.* 48, 40–58 (2010).

18 Van Rie A, Mupuala A, Dow A. Impact of the HIV/AIDS epidemic on the neurodevelopment of preschool-aged children in Kinshasa, Democratic Republic of the Congo. *Pediatrics* 122, E123–E128 (2008).

19 Cook-Easterwood J, Middaugh LD, Griffin WC 3rd, Khan I, Tyor WR. Highly active antiretroviral therapy of cognitive dysfunction and neuronal abnormalities in SCID mice with HIV encephalitis. *Exp. Neurol.* 205, 506–512 (2007).

20 Sosnik A, Chiappetta DA, Carcaboso A. Drug delivery systems in HIV pharmacotherapy: what has been done and the challenges standing ahead. *J. Control. Release* 138, 2–15 (2009).

21 Wong HL, Chattopadhyay N, Wu XY, Bendayan R. Nanotechnology applications for improved delivery of antiretroviral drugs to the brain. *Adv. Drug Del. Rev.* 62, 503–517 (2010).

▪▪ **Extensive review of the potential contributions of nanotechnology to improve antiretroviral therapy in the CNS.**

22 Kuo Y-Ch, Su FL. Transport of stavudine, delavirdine, and saquinavir across the blood–brain barrier by polybutylcyanoacrylate, methylmethacrylate-sulfopropylmethacrylate, and solid lipid nanoparticles. *Int. J. Pharm.* 340, 143–152 (2007).

23 Kuo Y-Ch, Kuo Ch-Y. Electromagnetic interference in the permeability of saquinavir across the blood–brain barrier using nanoparticulate carriers. *Int. J. Pharm.* 351, 271–281 (2008).

24 Chattopadhyay N, Zastre J, Wong HL, Wu XY, Bendayan R. Solid lipid nanoparticles enhance the delivery of the HIV protease inhibitor, atazanavir, by a human brain endothelial cell line. *Pharm. Res.* 25, 2262–2271 (2008).

25 Mishra V, Mahor S, Rawat A *et al.* Targeted brain delivery of AZT via transferrin anchored pegylated albumin nanoparticles. *J. Drug Target.* 14, 45–53 (2006).

26 Shaik N, Pan G, Elmquist WF. Interactions of pluronic block copolymers on P-gp efflux activity: Experience with HIV-1 protease inhibitors. *J. Pharm. Sci.* 97, 5421–5433 (2008).

▪ **Study describing the potentially beneficial effect of poly(ethylene oxide)–poly(propylene oxide) copolymers on the activity of efflux pumps in the CNS.**

27 Shaik N, Giri N, Elmquist WF. Investigation of the micellar effect of Pluronic P85 on P-glycoprotein inhibition: cell accumulation and equilibrium dialysis studies. *J. Pharm. Sci.* 98, 4170–4190 (2009).

▪ **Study describing the potentially beneficial effect of poly(ethylene oxide)–poly(propylene oxide) copolymers on the activity of efflux pumps in the CNS.**

28 Nowacek A, Gendelman HE. NanoART, neuroAIDS and CNS drug delivery. *Nanomedicine (Lond.)* 4, 557–574 (2009).

29 Sosnik A, Amiji M. Nanotechnology solutions for infectious diseases in developing nations. *Adv. Drug Del. Rev.* 62, 375–377 (2010).

30 Sosnik A. Nanotechnology contributions to the pharmacotherapy of pediatric HIV: a dual scientific and ethical challenge and a still pending agenda. *Nanomedicine (Lond.)* 5, 833–837 (2010).

31 Sosnik A, Carcaboso AM, Chiappetta DA. Polymeric nanocarriers: new endeavors for the optimization of the technological aspects of drugs. *Recent Pat. Biomed. Eng.* 1, 43–59 (2008).

32 Chiappetta DA, Sosnik A. Poly(ethylene oxide)–poly(propylene oxide) block copolymer micelles as drug delivery agents: improved hydrosolubility, stability and bioavailability of drugs. *Eur. J. Pharm. Biopharm.* 66, 303–317 (2007).

33 Sosnik A, Sefton MV. Semi-synthetic collagen/poloxamine matrices for tissue

doi:10.2217/NNM.12.104

engineering. *Biomaterials* 26, 7425–7435 (2005).

34 Sosnik A, Leung B, McGuigan AP, Sefton MV. Collagen/poloxamine hydrogels: Cytocompatibility of embedded HepG2 cells and surface attached endothelial cells. *Tissue Eng.* 11, 1807–1816 (2005).

35 Kurkalli BGS, Gurevitch O, Sosnik A, Cohn D, Slavin S. Repair of bone defect using bone marrow cells and demineralized bone matrix supplemented with polymeric materials. *Curr. Stem Cell Res. Ther.* 5, 49–56 (2010).

36 Fabbiani M, Di Giambenedetto S, Bracciale L *et al.* Pharmacokinetic variability of antiretroviral drugs and correlation with virological outcome: 2 years of experience in routine clinical practice. *J. Antimicrob. Chemother.* 64, 109–117 (2009).

37 Smith PF, Robbins GK, Shafer RW *et al.* Pharmacokinetics of nelfinavir and efavirenz in antiretroviral-naïve, human immunodeficiency virus-infected subjects when administered alone or in combination with nucleoside analog reverse transcriptase inhibitors. *Antimicrob. Agents Chemother.* 49, 3558–3561 (2005).

38 Marzolini C, Telenti A, Decosterd L, Biollaz J, Buclin T. Efavirenz plasma levels can predict treatment failure and central nervous system side effects in HIV-1-infected patients. *AIDS* 15, 1193–1194 (2001).

39 López-Cortés LF, Ruiz-Valderas R, Marín-Niebla A *et al.* Therapeutic drug monitoring of efavirenz: trough levels cannot be estimated on the basis of earlier plasma determinations. *J. Acquir. Immune Defic. Syndr.* 39, 551–556 (2005).

40 Peroni RN, Di Gennaro SS, Hocht C *et al.* Efavirenz is a substrate and in turn modulates the expression of the efflux transporter ABCG2/BCRP in the gastrointestinal tract of the rat. *Biochem. Pharmacol.* 82, 1227–1233 (2011).

41 Peroni RN, Hocht C, Chiappetta DA *et al.* The anti-HIV drug efavirenz is substrate and modulates the expression of the efflux transporter BCRP (ABCG2) in rats. Presented at: *First World Conference on Nanomedicine and Drug Delivery (WCN2010).* Kottayam, India, 19 October 2010.

42 Dutta T, Agashe HB, Garg M, Balasubramanium P, Kabra M, Jain NK. Poly (propyleneimine) dendrimer based nanocontainers for targeting of efavirenz to human monocytes/macrophages *in vitro*. *J. Drug Target* 15, 89–98 (2007).

43 Destache CJ, Belgum T, Goede M, Shibata A, Belshan MA. Antiretroviral release from poly(DL-lactide-co-glycolide) nanoparticles in mice. *J. Antimicrob. Chemother.* 65, 2183–2187 (2010).

44 Nowacek AS, Balkundi S, McMillan J *et al.* Analyses of nanoformulated antiretroviral drug charge, size, shape and content for uptake, drug release and antiviral activities in human monocyte-derived macrophages. *J. Control. Release* 150, 204–211 (2011).

45 Chiappetta DA, Hocht C, Taira C, Sosnik A. Efavirenz-loaded polymeric micelles for pediatric anti-HIV pharmacotherapy with significantly higher oral bioavailaibility. *Nanomedicine (Lond.)* 5, 11–23 (2010).

46 Chiappetta DA, Hocht C, Taira C, Sosnik A. Oral pharmacokinetics of the anti-HIV efavirenz encapsulated within polymeric micelles. *Biomaterials* 32, 2379–2387 (2011).

▪ **Reports the most extensive pharmacokinetic study of efavirenz-loaded polymeric micelles.**

47 Chiappetta DA, Alvarez-Lorenzo C, Rey-Rico A, Taboada P, Concheiro A, Sosnik A. N-alkylation of poloxamines modulates micellar encapsulation and release of the antiretroviral efavirenz. *Eur. J. Pharm. Biopharm.* 76, 24–37 (2010).

48 Chiappetta DA, Facorro G, Rubin de Celis E, Sosnik A. Synergistic encapsulation of the anti-HIV agent efavirenz within poly(ethylene oxide)-poly(propylene oxide) mixed polymeric micelles. *Nanomedicine* 7, 624–637 (2011).

49 Chiappetta DA, Hocht C, Sosnik A. A highly concentrated and taste-improved aqueous formulation of efavirenz for a more appropriate paediatric management of the anti-HIV therapy. *Curr. HIV Res.* 8, 23–31 (2010).

50 Mistry A, Stolnik S, Illum L. Nanoparticles for direct nose-to-brain delivery of drugs. *Int. J. Pharm.* 379, 146–157 (2009).

▪▪ **Updated review describing the nose-to-brain route.**

51 Dhuria SV, Hanson LR, Frey WH 2nd. Intranasal delivery to the central nervous system: mechanisms and experimental considerations. *J. Pharm. Sci.* 99, 1654–1673 (2010).

52 Kanazawa T, Taki H, Tanaka K, Takashima Y, Okada H. Cell-penetrating peptide-modified block copolymer micelles promote direct brain delivery via intranasal administration. *Pharm. Res.* 28, 2130–2139 (2011).

53 Cheng Q, Feng J, Chen J, Zhu X, Li F. Brain transport of neurotoxin-I with PLA nanoparticles through intranasal administration in rats: a microdialysis study. *Biopharm. Drug Dispos.* 29, 431–439 (2008).

54 Mainardes RM, Khalil NM, Gremião MP. Intranasal delivery of zidovudine by PLA and PLA-PEG blend nanoparticles. *Int. J. Pharm.* 95, 266–271 (2010).

55 Al-Ghananeem AM, Saeed H, Florence R, Yokel RA, Malkawi AH. Intranasal drug delivery of didanosine-loaded chitosan nanoparticles for brain targeting; an attractive route against infections caused by AIDS viruses. *J. Drug Target* 18, 381–388 (2010).

56 Jain R, Nabar S, Dandekar P *et al.* Formulation and evaluation of novel micellar nanocarrier for nasal delivery of sumatriptan. *Nanomedicine (Lond.)* 5, 575–587 (2010).

57 Illum L. Is nose-to-brain transport of drugs in man a reality? *J. Pharm. Pharmacol.* 56, 3–17 (2004).

58 Ribeiro A, Sosnik A, Chiappetta DA, Veiga F, Concheiro A, Alvarez-Lorenzo C. Single and mixed poloxamine micelles as suitable nanocarriers for solubilization and sustained release of ethoxzolamide for topical glaucoma therapy. *J. Royal Soc. Interface* (2012) (In Press).

59 Höcht C, Opezzo JA, Taira CA. Microdialysis in drug discovery. *Curr. Drug Discov. Technol.* 1, 269–285 (2004).

60 Höcht C, Lazarowski A, Gonzalez NN *et al.* Nimodipine restores the altered hippocampal phenytoin pharmacokinetics in a refractory epileptic model. *Neurosci. Lett.* 413, 168–172 (2007).

61 Maurin MB, Rowe SM, Blom K *et al.* Kinetics and mechanism of hydrolysis of efavirenz. *Pharm. Res.* 19, 517–521 (2002).

62 Rao KS, Reddy MK, Horning JL, Labhasetwar V. TAT-conjugated nanoparticles for the CNS delivery of anti-HIV drugs. *Biomaterials* 29, 4429–4438 (2008).

63 Prinsen BH, de Sain-van der Velden MG. Albumin turnover: experimental approach and its application in health and renal diseases. *Clin. Chim. Acta* 347, 1–14 (2004).

64 Liu J, Zeng F, Allen C. Influence of serum protein on polycarbonate-based copolymer micelles as a delivery system for a hydrophobic anti-cancer agent. *J. Control. Release* 103, 481–497 (2005).

65 Lo CL, Huang CK, Lin KM, Hsiue GH. Mixed micelles formed from graft and diblock copolymers for application in intracellular drug delivery. *Biomaterials* 28, 1225–1235 (2007).

66 Kabanov AV, Nazarova IR, Astafieva IV *et al.* Micelle formation and solubilization of fluorescent probes in poly(oxyethylene-*b*-oxypropylene-*b*-oxyethylene) solutions. *Macromolecules* 28, 2303–2314 (1995).

67 Southam DS, Dolovich M, O'Byrne PM, Inman MD. Distribution of intranasal instillations in mice: effects of volume, time, body position, and anestesia. *Am. J. Physiol.*

Lung Cell Mol. Physiol. 282, L833–L839 (2002).

68 van Rooy I, Cakir-Tascioglu S, Hennink WE, Storm G, Schiffelers RM, Mastrobattista E. *In vivo* methods to study uptake of nanoparticles into the brain. *Pharm. Res.* 28, 456–471 (2011).

69 de Lange EC, de Boer BA, Breimer DD. Microdialysis for pharmacokinetic analysis of drug transport to the brain. *Adv. Drug Deliv. Rev.* 36, 211–227 (1999).

70 Gaucher G, Satturwar P, Jones MC, Furtos A, Leroux JC. Polymeric micelles for oral drug delivery. *Eur. J. Pharm. Biopharm.* 76, 147–158 (2010).

71 Balani SK, Kauffman LR, deLuna FA, Lin JH. Non-linear pharmacokinetics of efavirenz (DMP-266), a potent HIV-1 reverse transcriptase inhibitor, in rats and monkeys. *Drug Metabol. Disp.* 27, 141–145 (1999).

72 Wohlfart S, Gelperina S, Kreuter J. Transport of drugs across the blood–brain barrier by nanoparticles. *J. Control. Release* 161(2), 264–273 (2012).

73 Petri B, Bootz A, Khalansky A *et al.* Chemotherapy of brain tumour using doxorubicin bound to surfactant-coated poly(butyl cyanoacrylate) nanoparticles: revisiting the role of surfactants. *J. Control. Release* 117, 51–58 (2007).

74 Alvarez-Lorenzo C, Rey-Rico A, Brea J, Loza MI, Concheiro A, Sosnik A. Inhibition of P-glycoprotein pumps by PEO–PPO amphiphiles: branched versus linear derivatives. *Nanomedicine (Lond.)* 5, 1371–1383 (2010).

75 Cuestas ML, Sosnik A, Mathet VL. Poloxamines display a multiple inhibitory activity of ATP-Binding Cassette (ABC) transporters in cancer cell lines. *Mol. Pharm.* 8, 1152–1164 (2011).

76 Cuestas ML, Castillo A, Sosnik A, Mathet VL. Inhibition of the functional activity of diverse ABC pumps by poloxamines in hepatic cell lines. Presented at: *XVI Argentine Congress of Hepatology*. Buenos Aires, Argentina, 9–11 June 2011.

77 Lourenço Cardoso F, Brites D, Brito MA. Looking at the blood–brain barrier: molecular anatomy and possible investigation approaches. *Brain Res. Rev.* 64, 328–363 (2010).

78 Dhanda D, Frey WH 2nd, Leopold D, Kompella UB. Approaches for drug deposition in the human olfactory epithelium. *Drug Deliv. Technol.* 5, 64–72 (2005).

79 Zhang QZ, Zha LS, Zhang Y *et al.* The brain targeting efficiency following nasally applied MPEG-PLA nanoparticles in rats. *J. Drug Target* 14, 281–290 (2006).

Website

101 AIDS epidemic update 2009, World Health Organization. www.who.int/hiv/epiupdates/en/index.html

doi:10.2217/NNM.12.104